Analyst

A Capillary Flow-Driven Microfluidic System for Microparticle-Labeled Immunoassay

Journal:	*Analyst*
Manuscript ID	AN-ART-05-2018-000898
Article Type:	Paper
Date Submitted by the Author:	14-May-2018
Complete List of Authors:	KhodayariBavil, Ali; Texas Tech University, Mechanical Engineering Kim, Jungkyu; Texas Tech University, Mechananical Engineering;

SCHOLARONE™
Manuscripts

A Capillary Flow-Driven Microfluidic System for Microparticle-Labeled Immunoassay

Ali Khodayari Bavil and Jungkyu Kim*

Department of Mechanical Engineering, Texas Tech University, Lubbock, TX

* Address correspondence to: Jungkyu (Jay) Kim

Department of Mechanical Engineering

Texas Tech University

Lubbock, Texas 79409, USA

Phone: (806) 834-6106

E-mail: jungkyu.kim@ttu.edu

Abstract

A simple, reliable, and self-powered capillary flow-driven microfluidic platform is developed for conducting microparticle-labeled immunoassays. To obtain the washing forces and binding kinetics appropriate for microparticle-labeled immunoassays, both microchannel networks and sample access holes are designed and characterized to confirm the fluidic routes. To demonstrate two different types of immunoassays, serial and parallel capillary-driven microfluidic platforms were developed for mouse immunoglobulin G (IgG) and cardiac troponin I (cTnI) using detection antibody-conjugated microparticles, respectively. Using the serial capillary-driven microfluidic platform, we successfully demonstrated IgG quantification using direct immunoassay and achieved a limit of detection (LOD) of 30 pM by using pre-immobilized mouse IgG. In the parallel capillary-driven microfluidic platform, a sandwich immunoassay for detecting cTnI was demonstrated and a clinically relevant LOD as low as 4.2 pM is achieved with minimal human intervention. In both assays, the association rate constants (K_a) are measured to estimate the overall assay time. According to these estimations, microparticle-labeled immunoassays could be conducted in few minutes using the proposed capillary-driven microfluidic devices. By coupling with various magnetic sensors, these simple immunoassay platforms enable us to achieve a true sample-in-answer-out device that can screen for a variety of targets without relying on external power sources for fluidic manipulation.

Keywords: Microfluidics, Capillary-driven flow, Microparticle-labeled immunoassay, Binding kinetics, Point-of-care diagnostics

1. Introduction

A microfluidic device allows small volumes of target samples and reagents to be used for a variety of biological and chemical screenings. However, to control flow precisely, most microfluidic devices rely on active fluid-control systems, such as syringe pumps, centrifuges, and electrical and mechanical actuators[1-5]. Though active systems enable the accurate manipulation of nano- and pico-liter samples, they can be impractical for point of care (POC) diagnostics due to their high-power requirements, multiple fabrication steps, and complex controlling circuits. Recently, much effort has been devoted to developing passive transport mechanisms such as hand-power devices[6-8], pre-vacuumed[9, 10] and capillary driven microfluidics[11-15], that can simplify overall microfabrication and microfluidic operation, rendering microfluidic platforms highly portable and versatile overall. By incorporating passive transport mechanisms, highly practical POC screening platforms can be developed by coupling various sensing tools to isolate and identify various biomolecules.

Among passive control systems, capillary flow-driven systems are the most attractive approach due to cost-effective fabrication and simple fluidic operations. Various capillary-flow-driven systems have been introduced to isolate plasma, detect various biomarkers, and enable the autonomous, simple, and controlled manipulation of liquids. A multi-parametric microfluidic chip that allows a one-step immunoassay is developed for C-reactive protein (CRP)[12]. First, detection antibodies (dAbs) and 20 μL of human serum were combined in the Dean flow mixer. This mixture was then analyzed in 6 parallel microchannels, each of which produced a different level of hydraulic resistance and thus a different reaction time. Although this microfluidic chip is well-designed, the assay results are highly dependent upon the success of a washing function to remove unspecific bindings. Moreover, a fluorescent scanner is required to obtain the assay results, which limits the portability of this assay platform. Another capillary-driven microfluidic immunoassay was introduced using an embedded optical component in a single microchannel that measures the fluorescence intensity to detect cardiac Troponin I (cTnI)[15]. This platform achieved a good sensitivity with 24 pg mL^{-1} with a standard sandwich immunoassay procedure. However, it has limited scalability to increase overall throughput since parallel sensing by splitting or controlling exciting beam using the embedded micro-lens can decrease sensitivity and portability.

A microparticle-labeled assay has been developed that is equally sensitive to a standard fluorescence technique and does not require any complex fluorescent detectors. This assay format was recently used to detect Tetrodotoxin (TTX)[16] , Hepatitis B surface Antigen (HBsAg)[17], Human IgG[18], and Tumor Necrosis Factor-α (TNF-α)[19]. In general, target molecules were covalently immobilized on a substrate which was mounted onto a compression-sealed fluid cartridge featuring a macroscale valve and flow cells connected to a peristaltic pump for fluidic manipulation. A mixture of target molecules and dAb-coated microparticles were then pumped onto the surface of the substrate and the surface coverage of the microparticles was measured to quantify the target molecules. One of the key challenge is to minimize non-specifically bound microparticles to achieve highly sensitive immunoassay. Previous studies found that hydrodynamic forces between 0.1 and 10 pN can rupture non-specific bonds and that those between 6 and 250 pN preserve specific bonds[20-22]. Exploiting the controlled hydrodynamic forces imposed by the flow velocity, non-specifically bound microparticles were removed from the detection area to increase the signal to noise ratio[19]. Even though these assay demonstrations achieved relatively good LOD, bulky fluidic control systems were used to handle the samples and reagents. To improve the sample handling of these microparticle-labeled immunoassays, an automated microfluidic device was developed that improves sample delivery by using controlled hydrodynamic washing to remove unspecific bindings[3]. The resulting platform was used to conduct two different immunoassays for mouse IgG and human prostate specific antigen with limits of detection of 1.8 and 3 pM, respectively. Despite the advantages of this platform, however, the difficulty of fabricating the multilayered microchip and external pneumatic system limited its use in POC diagnostics.

In this study, we designed a capillary-driven microfluidic device that uses a bridging hole between the inlet and the outlet to deliver analytes and washing solutions automatically and sequentially. To obtain the necessary sensitivity, we examined flow characteristics and calculated the hydrodynamic force on biomolecules on both serial and parallel designs. To validate these devices, we conducted microparticle-labeled immunoassays using small volumes (~1 μL) of analytes to detect mouse IgG and cTnI by determining the surface coverage of microparticles. We achieved the association constant and relevant LOD for mouse IgG and cTnI. This simple, capillary-driven microfluidic platform can be used to conduct a variety of bioassays by integrating with biosensors in settings with limited access to laboratories.

2. Design and working principle

As shown in **figure 1A and 1B,** two passive microfluidic devices which are a serial capillary-driven microfluidics (SCM) and parallel capillary-driven microfluidics (PCM) are designed for direct and sandwich immunoassays, respectively. Both devices have three functional sections. The *buffer priming section* (1) contains buffer solution for washing and is filled via the inlet hole (D = 2.5 mm). The *assay section* (2) is where the assay occurs and contains antibody-functionalized patterns. The *waste-bin* (3) holds all samples and reagents while the assay is completed. A sample-in hole (D = 0.5 mm) between the inlet and the outlet allows for the sequential delivery of analyte and buffer solutions. By connecting multiple microchannels using the similar design concept, precisely designed branches in the PCM produce equal hydraulic resistance in each branch. To load multiple target samples, the PCM has multiple sample-in holes as well as a dAb-delivery hole for detection antibody-conjugated microparticles. The meandering design of the channels in both the buffer priming section and the assay section allows the device to be miniaturized. The channel in the buffer priming section has a fixed width of 500 μm and a length of 80 mm, allowing it to accommodate a sufficient volume of buffer solution while maintaining low hydrodynamic resistance. In contrast, the channel in the assay section has a width of 200 μm, which is small enough to minimize the required analyte volume and to keep the velocity in the desired range.

Initially, the priming section are filled with phosphate-buffered saline with 1% w/v bovine serum albumin (BSA), PBSB, up to the sample-in hole(s). For SCM described in **Figure 1A** with the height of 120 μm, by loading 20 μL PBSB via the inlet, the buffer can cover a distance of 35 mm after the sample-in hole due to the capillary force and the upstream hydraulic pressure. Passing PBSB buffer through the sample-in hole accomplishes the dynamic adsorption of BSA to simplify passivation of the channel surfaces in the assay section[23]. Once the SCM is primed, 1.5 μL of detection antibody-conjugated microparticles is loaded via the sample-in hole and the tape on the outlet is removed to perform direct immunoassay. Detailed procedure for SCM can be found in **ESI video S1**. For PCM having height of 90 μm, by priming with the same procedures, each of four branches are covered with the same length of 44 mm with PBSB. Then, four different concentrations of the target and detection antibody-conjugated microparticles are introduced via the sample-in holes and the dAb-delivery hole, respectively as shown in **Figure 1B**. By detaching the tape, the loaded target samples, the conjugated microparticles, and the

buffer solution are sequentially delivered into the assay section and transported into the waste-bin. This sequence allows the formation of immunocomplex and remove unbounded target samples and microparticles by washing with the buffer solution. Overall procedure can be found in **ESI video S2**, demonstrating all sandwich immunoassay protocols.

3. Materials and methods

Device fabrication

A microfluidic channel was created using conventional soft lithography. First, the microchannel was modelled in AutoCAD and a photomask for UV exposure was purchased (CAD/Art Services, Inc., USA). Next, SU-8 2035 (MicroChem Corp., USA) was dispensed onto four silicon wafers (Addison Engineering Inc., USA) and spin coated at different speeds to obtain channel heights of 30 µm, 60 µm, 90 µm, and 120 µm. The wafers were then sequentially soft baked at 65 ºC and 95 ºC and exposed to UV light (UV-KUB 2, France) through a PL-360LP optical filter (Omega Optical Inc., USA) to create straight sidewalls for the microchannel. The wafers were then baked again at 65 ºC and 95 ºC for a post-exposure bake. The microchannel pattern was developed using SU-8 DEV (MicroChem Corp., USA). Poly-(dimethylsiloxane) (PDMS) pre-polymers (Sylgard 184, Dow Corning, Midland, MI) and a curing agent were mixed in a 5:1 ratio, which provides relatively low surface roughness and air permeability compare to normal 10:1 ratio[24, 25], and poured into the SU-8 mold. To complete the polymerization of the PDMS, the mold was cured on a hot plate for 60 minutes at 100 ºC and stored in an oven overnight at 65 ºC. After all of wells were punched onto the PDMS replica with various sized biopsy punchers, the replica was permanently bonded to a glass slide after the oxygen plasma treatment. This fabrication process is detailed in **ESI figure S1**.

Hydrodynamic forces

To ensure that a microparticle-labeled immunoassay is highly sensitive, the surface of the substrate should be washed with a hydrodynamic force sufficient to remove unspecific microparticles. Assuming a uniform laminar Poiseuille flow, the flow velocity from the plane wall at bead radius (a) is estimated by:

$$v_{z=a} = V \times \frac{6a}{h} \qquad (1)$$

, where V is the bulk velocity and h is the channel height[3]. On the Stokes formulation of uniform flow, the force (F) and the torque (T) on a bead are estimated, respectively, by $F_s = 6\pi\eta a v$ and $T_s = 4\pi\eta a^2 v$, where $\eta = 1mPa.s$ is the dynamic viscosity of the fluid. Because a tether length is very small compared to a microparticle, shear-induced force and torque both approach finite limits as a microparticle contacts a wall. These limits can be estimated by $F = 1.70 \times F_s$ and $T = 0.944 \times T_s$, respectively[26]. The microparticle tether acts as a lever, exposing the microparticle to repercussion torque. The hydrodynamic shear force on the microparticle is magnified by the ratio of its radius to its distance from the wall (see **ESI figure S2**). The force applied by the fluid is coincident with the torque introduced by the tether, so the total force can be approximated by:

$$F_{tether} \cong \left(F + \frac{T}{a}\right)\sqrt{\frac{a}{2L}} \qquad (2)$$

, where L is the length of the tether[20]. Since the magnitude of this force on the particles is highly dependent on flow velocity, further investigations are required to obtain flow velocity associated with microchannel geometry in capillary-driven microfluidic platforms.

Flow characterization of capillary-driven microfluidics

The flow behaviors of the sample and buffer solutions in the channel are the key parameters in performing a microparticle-labeled immunoassay. In a capillary-driven flow, the cross section of the channel, the fluid viscosity, and the surface tension also affect the flow rate. To achieve an optimized channel aspect ratio, we measured only the time-dependent velocities for different channel heights, fixing the other parameters. To do so, we recorded the flow at 60 fps and tracked the flow meniscus using a homemade MATLAB code, which is shown in **ESI figure S3**.

Microparticle labeled immunoassay

Surface preparation: A slide-glass substrate was selectively bio-functionalized with the antibody using carbodiimide-induced cross-linking (**figure 2**). The glass slide was first cleaned by treating it for 15 minutes with freshly prepared piranha solution—which consisted of a 2:1 ratio of H_2SO_4 (97.5%, v/v) and H_2O_2 (30%, v/v)—rinsing it extensively with de-ionized (DI) water, and

nitrogen drying it. A patterned PDMS film (HT6240, Rogers Corporation, USA) was used as a mask for surface functionalization, and the area exposed to air was treated with oxygen plasma to promote hydroxylation. The surface was then treated with a 5% (3-Aminopropyl) triethoxysilane (APTES) in deionized (DI) water for 30 minutes to produce self-assembled monolayers (SAMs) containing amino-functionalized sites. After the slide was washed with DI water and the APTES-treated regions were nitrogen dried, the slide was stored in a desiccator until it was used.

Demonstration for mouse IgG: As a preliminary confirmation of this device, we used the SCM to conduct a simple direct immunoassay for mouse IgG. The surface of the glass substrate was functionalized with 6 different concentrations of mouse IgG that ranged from 500 μg mL^{-1} to 5 ng mL^{-1} and were obtained using a 10-fold dilution in PBS. First, the mouse IgG antibody (Thermo-Fisher Scientific Inc., USA) was immobilized using the 1-Ethyl-3-(3-dimethylaminopropyl) carbodiimide (EDC) and N-hydroxysuccinimide (NHS)–based carbodiimide coupling method. After the antibodies were activated with EDC–NHS, they were incubated for 40 minutes on amine-functionalized patterns. All excess antibodies were then extensively washed with PBS.

To prepare antibody-conjugated microparticles, 1 μm sized magnetic microparticles (MyOne Streptavidin T1, Thermo-Fisher Scientific Inc., USA) were washed three times in PBS with Tween-20 (PBST, 0.1% v/v). 2 μL of microparticles were then mixed with 50 μL of 7 μg mL^{-1} biotinylated goat anti-mouse IgG (Abcam Inc., USA) and gently rotated for 30 minutes at room temperature. The anti-mouse IgG conjugated with magnetic microparticles was washed three times with PBST (1% Tween-20) to ready it for use in the microparticle-labeled immunoassay. To demonstrate that the immunoassay can detect mouse IgG, 1μL of the microparticles conjugated with biotinylated anti-mouse IgG was introduced through the sample-in hole. The sample was automatically delivered to the assay section when the cover tape was removed from the outlet. This hydraulic washing simultaneously regulated the capillary flow, delivered the sample, and removed any unbound microparticles from the surface of the substrate. The assay was completed in only 3 minutes.

Immunoassay for cardiac Troponin I: The device's capacity for sandwich immunoassay was demonstrated by using it to detect cardiac Troponin I (cTnI) on PCM. A capture antibody (cAb), monoclonal anti-cardiac Troponin I (ab10231, Abcam Inc., USA) was diluted with PBS to make

500 μg mL^{-1} and immobilized on the glass surface indicated in Figure 1 via the carbodiimide coupling method described above. Human cardiac Troponin I (ab207624, Abcam Inc., USA) was diluted with PBS (using 100-fold dilutions) to obtain four different concentrations ranging from 100 μg mL^{-1} to 0.1 ng mL^{-1}, and these concentrations were loaded through the sample-in holes. 500 μg mL^{-1} of anti-cardiac Troponin I antibody (ab47003, Abcam Inc., USA) was conjugated to 2.8 μm magnetic microparticles using Dynabeads Antibody Coupling Kit (Thermo Fisher Scientific, USA). 1 μL of conjugated microparticles was loaded through the detector-delivery hole. When the tape on the outlets was removed, the troponin I and the microparticles passed sequentially over the capture-antibody-coated assay section and were followed by a stream of washing solution.

Binding kinetics: During the microparticle immunoassay, the association/dissociation reactions[27] for the different concentrations of analytes were evaluated under the capillary flow using a programmable, motorized-stage optical microscope. First, the coordinates of patterned spots on the surface, the length of the video acquisition, the number of repetitions, and the total time of the experiment were coded into the imaging software that controlled the NIS-Elements microscope (Nikon Ti-E, Japan). Then, starting the assay, we ran the NIS manipulation program and analyzed the extracted frames of the recorded videos using the image processing feature of the software. The number of beads at a chosen spot was measured every 40 seconds, and these measurements were plotted against the reaction time to obtain the association constants for each assay.

4. Results and discussion

Characterization of capillary-driven flow

Both theoretical and experimental studies were performed on the SCM to characterize its capillary-driven flow. Haigen-Poiseuill's law dictates that in a rectangular cross section of a microchannel $Q = \frac{h^3 w \Delta p}{12 \eta L}$, where η is the fluid viscosity[28]. The capillarity-induced pressure drops in the channel between the entrance and the meniscus are described by the Young-Laplace equation, $\Delta p = \gamma.(\frac{\cos\theta_T + \cos\theta_B}{h} + \frac{\cos\theta_R + \cos\theta_L}{w})$, in which γ is the surface tension between the liquid and the air and θ_T , θ_B, θ_R and $\theta_L$are the contact angles at the top, bottom, right and left

side of the channel, respectively. Since, the wetting of a PDMS surface is dependent on time after oxygen plasma treatment[29], all experiments were conducted within 30 minutes of oxygen plasma activation to minimize experimental variation. When the gravitational force is neglected, the velocity in the horizontal capillary-pump is found by replacing $Q = \frac{dl}{dt}wh$ with:

$$V(t) = \frac{dL(t)}{dt} = \sqrt{\frac{\gamma \,.\, h^2}{24\,\eta\,.t}\left(\frac{\cos\theta_T + \cos\theta_B}{h} + \frac{\cos\theta_R + \cos\theta_L}{w}\right)} \qquad (3)$$

As expected from equation (3), overall velocity profiles in the buffer priming section shown in **Figure S4** decreased exponentially with time from the initial flow velocity of respective channel height. The velocity profiles at transient stages show less reliable flow velocity and then become steady over time. Even though there are some inevitable variations on PDMS surface mostly caused by time-dependent surface wetting properties and inhomogeneous surface charge density after oxygen plasma treatment, these velocity profiles show relatively good agreement with the theoretical **Equations (3)** which verifies the height-dependency of velocity.

The average velocity in the assay section was investigated with respect to various channel heights as well. In the assay section, antibodies were selectively immobilized onto the substrate by masking with a PDMS film having multiple square-shaped openings. The area contacting with the PDMS film increases its hydrophobicity and other antibody-functionalized surface increases its hydrophilicity[30]. In this way, the flow velocity was increased on the functionalized surface while the surface was wetted by the washing solution. Even though only the surface of the glass substrate was modified, these phenomena increased a flow velocity up to 10% on functionalized patterns. By passing the buffer solution over the functionalized patterns, the ultimate average velocity becomes stable in the assay section and falls to 2, 3, and 5.5 mm s^{-1} for channel heights of 60, 90 and 120 μm, respectively.

Table 1: Hydrodynamic forces for microparticle-labeled immunoassays

Microparticle diameter [μm]	Channel cross section [μm×μm]	Average velocity in the channel [mm/s]	Force on the bead [pN]	Total Force [pN]
2.8	850 × 70	0.22	1.2	24-30 [3]
2.8	250 × 60	6.66	-	60 [19]
1.0	200 × 120	5.5	2.2	10
2.8	200 × 90	3	12	94

Demonstration of the microparticle-labeled assay

With this working principle, two microparticle-labeled immunoassays were performed to quantify mouse IgG and cTnI on SCM and PCM, respectively. Key goals for a microparticle-labeled immunoassay are to effectively deliver microparticles to antibody-coated areas to maximize binding kinetics and to control hydrodynamic washing to remove unbound microparticles. To achieve the proper binding kinetics between the analytes and the capture antibodies—thereby achieving a high ratio of signal to noise—we designed the microchannel geometry to generate an appropriate hydrodynamic force under the capillary-driven flow.

According to equation (2), 1 μm and 2.8 μm microparticles in channels with heights of 120 μm and 90 μm with a tether length of roughly 20 nm can have 10 and 94 pN, respectively, shown in **table 1** including previous studies. The total forces are less than the adhesion strength in the immunocomplex, however, they are sufficient to dislodge nonspecific bindings from the surface. Since the flow velocity was regulated for microparticle delivery and any unbound microparticles were removed from the surface of the substrate effectively, association and dissociation of immunocomplex formation occurred effectively in the absence of any extra hydrodynamic-washing steps. To confirm this, the association rate constant (K_a) and the dissociation rate constant (K_d) were studied to determine the binding affinity ($k = \frac{k_a}{k_d}$) of the target. Determining the binding affinity of the target, in turn, yielded information about the intermolecular interactions and the binding strengths in the biomolecule complex and about how it forms and breaks down over time[31]. Optical technologies are preferable for measuring binding affinities because they allow direct detection and real-time monitoring. When the kinetics of the antigen–antibody interaction were assessed using a fluorescence-based biosensor, the results

indicated that for channel widths larger than ~200 nm, reducing the width of the spot does not significantly affect the association rate between the antigen and the immobilized antibody[32]. Surface plasmon resonance (SPR), another optical detection technique, is also commonly used to measure molecular binding interactions. Although this techniques is label-free and precise, it requires a specific setup with a processor and demonstrates a mass transport limitation[27]. A magnetic-bead-based ligand binding assay was recently introduced that uses mass spectrometry to detect human kynurenine 3-monooxygenase (KMO)[33]. This robust technique requires a chromatographic system and can take up to 4 hours. In contrast, we used only binding kinetics to investigate the association rate for an immune complex in a few minutes.

Number of the microparticles were normalized with the final values for the various concentrations of mouse IgG (which ranged from 500 μg mL^{-1} to 5 ng mL^{-1}) and plotted versus time, as is shown in **figure 3A.** As was previously discussed, the fitted sigmoid curve reveals an association rate that is initially low because the high velocity of the capillary flow that increases reaction limitation[34]. Numerical studies have shown that high flow velocities improve surface binding by reducing the mass transport limitation[35]. Low flow velocities, in contrast, increase analyte exploitation by extending the assay time. Therefore, the overall binding of the microparticles increases considerably 25 seconds after the analytes are introduced; the surface coverage exceeds 90 percent of its final value after 3 minutes. **Figure 3B** shows the real-time, normalized particle densities during the assay for different concentrations of cTnI, which ranged from 100 μg mL^{-1} to 100 pg mL^{-1}. These results indicate that the affinity rate in this capillary-driven system is independent of the target concentration of the immobilized antibody; the target sample diffuses throughout the assay section within a few seconds because of the high flow velocity at the start of sample delivery. Then, as the flow velocity decreases over time, the association rate increases, and equilibrium is achieved. This occurs in the same amount of time for different concentrations of the target antibody. **Figure 3** reveals average association rates of around 4.75×10^5 M^{-1} S^{-1} and 88.18×10^5 M^{-1} S^{-1} were found for anti-mouse IgG and anti-human cTnI, respectively. Since washing occurs during the same step as does sample adsorption, dynamic binding occurs and there is no separate dissociation phase after surface saturation. It should be noted that the equilibrium constant is different for each concentration since **figure 3** shows the normalized value by final surface density for each concentration. This real-time microscopy technique simultaneously detects antibodies tagged with microparticles and

measures the binding affinity without relying on any complicated biosensors[31] or special surface modifications[27]. Since analytes are labeled with microparticles, the affinity rate for a given biomolecule complex can be determined by calculating the hydrodynamic forces on the beads and selecting the proper flow rate.

To evaluate the sensitivity, the portion of a given surface covered with microparticles was calculated for each concentration of mouse IgG and cTnI and the results are shown in **figure 4**. When used to perform the assays, our device obtained a limit of detection as low as 5 ng mL^{-1} (equal to 30 pM) for mouse IgG and 0.1 ng mL^{-1} (equal to 4.2 pM) for cTnI. Unlike similar microfluidic devices that require fluorescent light to read, our device requires only conventional optical microscopy. The standard curve of sensitivity generally shows log-linear dependency on target concentration. Due to the sequence of the surface patterns (see **ESI figure S5**), however, a slight change in the slope of bead density to target concentration is observed between 5 and 0.5 μg mL^{-1} for mouse IgG as is shown in **figure 4**. Despite the favorable LOD of this device, which is in the clinically relevant range[36], a slightly lower curve slope is observed than with traditional ELISA immunoassays. This can be explained by two factors: spontaneous dilution phenomena and the low incubation time for the target required by this device. It should be noted that because a back-flow regime occurs after the target is dispensed in the parallelized design, the target dilutes spontaneously before it flows over the functionalized area. Additionally, it is crucial that patients affected by cardiac disease quickly seek proper triage and treatment in the early stages of the disease[36]. Instead of taking hours, as it does with the standard ELISA assay, cTnI detection takes less than 10 minutes (including a 1-minute incubation time) with this device.

5. Conclusion and prospects

We introduce a novel, easy-to-use, and fast-response passive microfluidic platform for microparticle-labeled immunoassays. This device uses capillary-driven flow to precisely control flow velocity and maximize mass transport, forming an immune complex and performing hydrodynamic washing without an external energy source. Different channel aspect ratios produce different flow velocities and exert different amounts of drag force on the microparticles. To achieve a proper range of hydrodynamic force, the appropriate channel geometry selected for each assay. Two immunoassays are conducted on two platforms of SCM and PCM to quantify mouse IgG and cTnI, respectively. To determine the binding kinetics, the surface coverage was

monitored during the assay and plotted versus time to estimate the affinity for various target concentrations. From these demonstrations, we confirmed that this unique platform can be extended to a variety of immunoassay formats by simply replacing the antibody types and adding additional parallel channels for multiple sample-in holes. By coupling with sample preparation systems and magnetic sensors, this platform can move one step closer to a real sample-in answer-out system. Previously, we successfully demonstrated a serum separator to perform immunoassay and glucose tests using Vivid Plasma Separation GX membrane (Pall Life Sciences, USA)[37]. By embedding this membrane onto sample inlets[38], one-step serum separation can be implemented to improve practicality of this capillary-driven microfluidic immunoassay platform. Furthermore, miniaturized downstream biosensors can be used to measure surface coverage of magnetic particles instead of a bulky optical microscope. Due to simplicity of this device, the platform can be integrated with Giant Magnetoresistance (GMR)[39, 40] or Hall-effect bead detectors[41, 42] to achieve a biosensing platform for resource-limited settings.

One of the key challenge for a capillary-driven microfluidic device is to maintain surface wetting property to obtain excellent repeatability of immunoassays. This can be achieved by using surface modification techniques or alterative materials. A layer-by-layer (LBL) deposition of positively and negatively charged species followed by aqueous NaCl solution[43], deposition of polyvinyl alcohol following plasma treatment[44] or poly(ethylene glycol) coating produce long-term stable hydrophilic surface for PDMS channels. Additionally, different polymeric materials such as polycarbonate (PC), poly- methyl-meta-acrylate (PMMA), cyclic olefin copolymer (COC) and polyimide have been introduced to overcome the innate drawbacks of PDMS[45]. Utilizing these techniques will change the flow velocity regime due to different surface wettability. Further flow characterization should be elaborated to determine a range of the flow rate for implementing microparticle-labeled immunoassays effectively.

Acknowledgements

This research was primarily supported by National Science Foundation Grant NSF-EECS/1509746. J. Kim would like to thank Texas Tech University for its financial support of this project with new-investigator start-up funding.

Figures

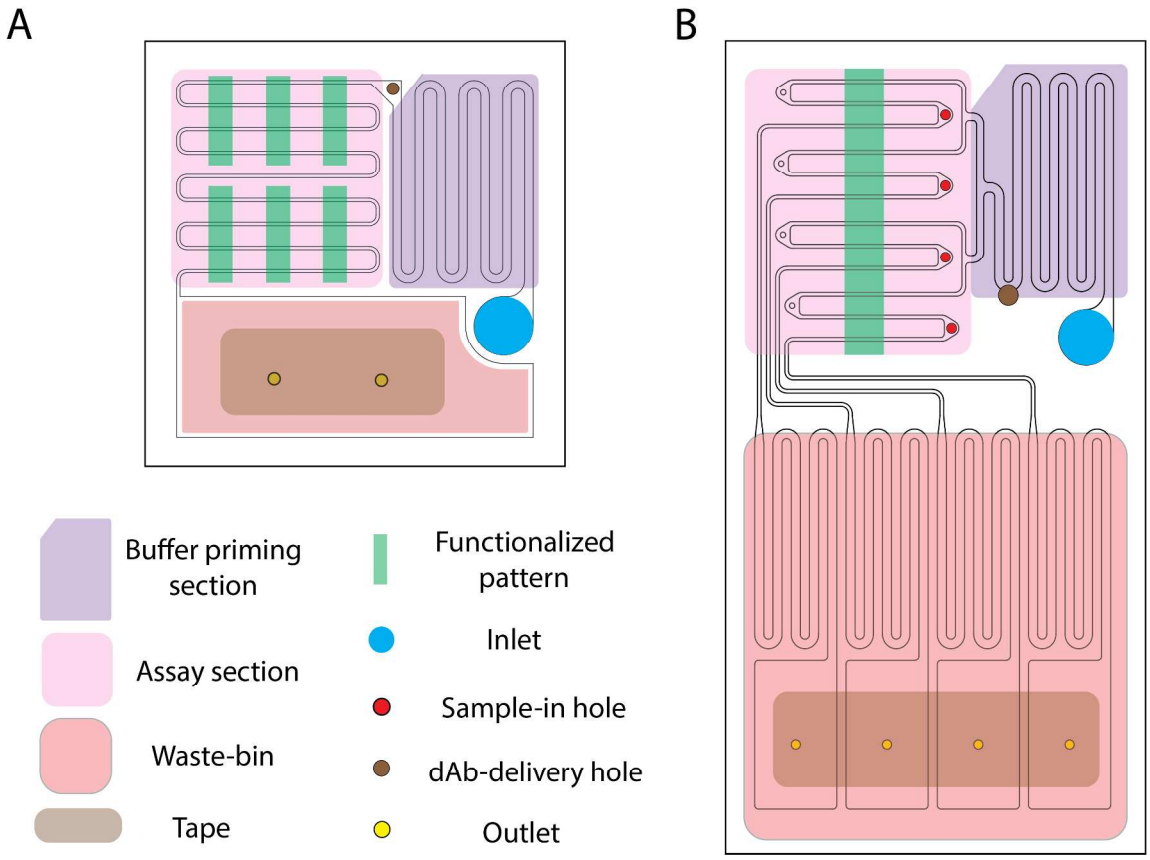

Figure 1. Description of a capillary-driven microfluidics device for microparticle-labeled immunoassays. (A) Design for a direct immunoassay. (B) Parallelized-design for a sandwich immunoassay.

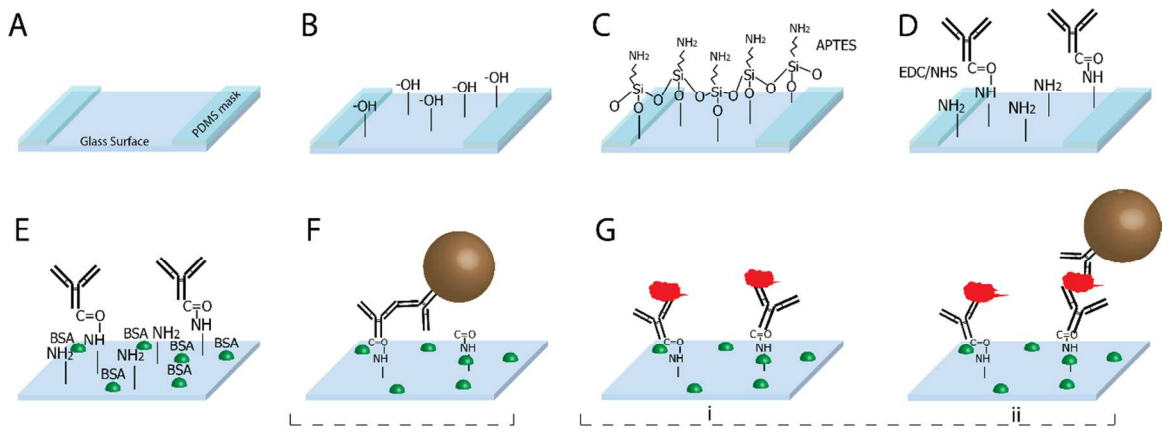

Figure 2. Surface functionalization and biochemistry. (A) The glass slide is cleaned with piranha solution and covered with a patterned PDMS film. (B) The substrate is treated with oxygen plasma to promote hydroxylation. (C) The hydroxylated surface is functionalized using a 5 % (3-Aminopropyl) triethoxysilane (APTES) solution. (D) Antibody immobilization chemistry is introduced via the EDC and NHS-based heterobifunctional crosslinking method. (E) After the PDMS is bonded to the glass substrate, PBSB is introduced into the microchannel. (F) In the serial design, biotinylated anti-mouse IgG conjugated with streptavidin-coated microparticles is introduced via the microfluidic channel. (G) In the parallelized-design: i. cTnI incubation on cAb. ii. dAb conjugated with microparticles flows over the patterned area to complete the immunocomplex.

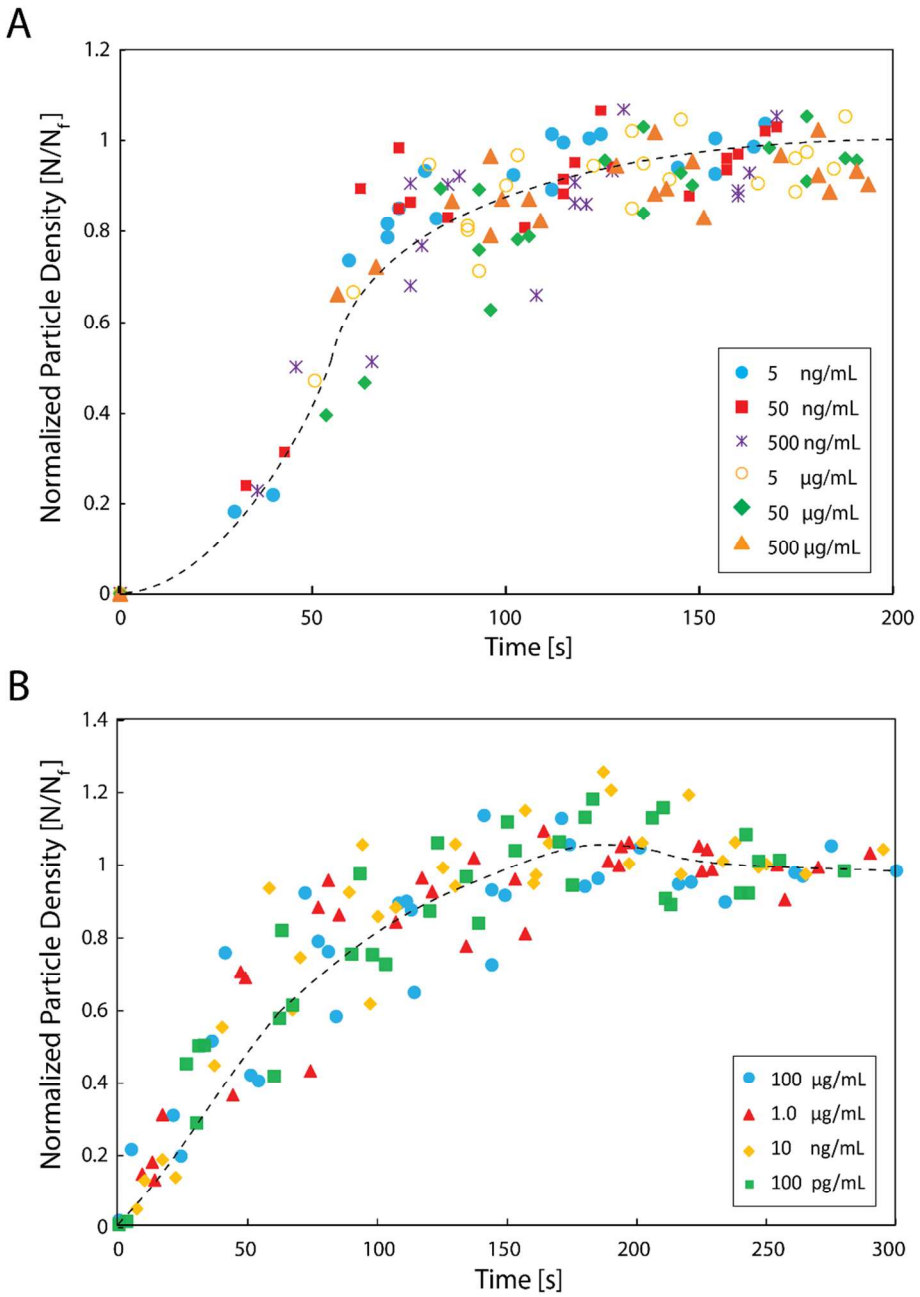

Figure 3. Kinetic analysis of the binding using the normalized bead number (the ratio of the bead number to the final number of beads) versus time for (A) mouse IgG and (B) cTnI. N and N_f are the number of microparticles at time and final, respectively.

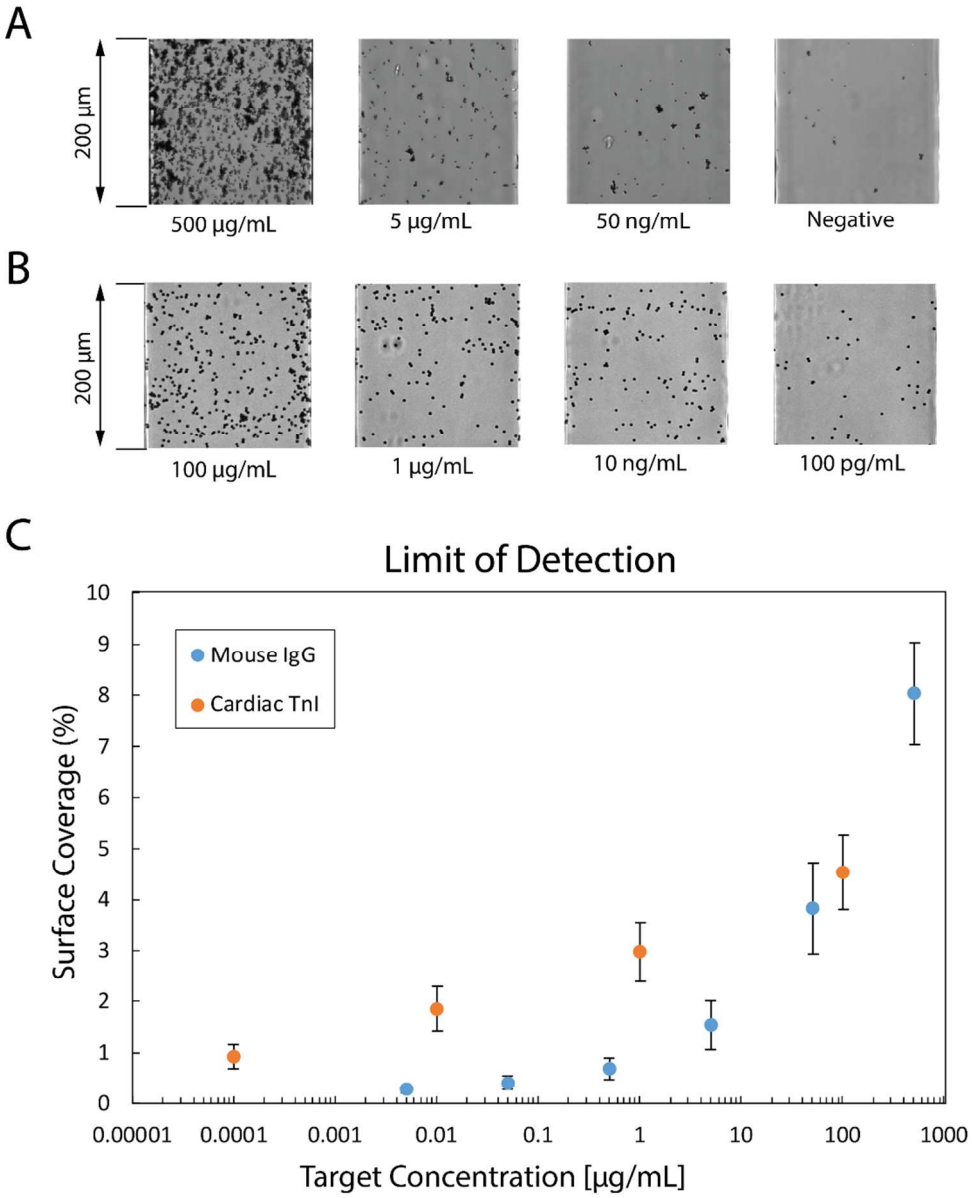

Figure 4. The bead populations (A) for mouse IgG and (B) for cardiac Troponin I. (C) The limit of detection for mouse IgG and cTnI is plotted as the bead density (number of detectors per area) versus the target concentration.

References

1. M. Behnam, G. V. Kaigala, M. Khorasani, P. Marshall, C. J. Backhouse and D. G. Elliott, *Lab Chip*, 2008, **8**, 1524-1529.
2. R. Sista, Z. Hua, P. Thwar, A. Sudarsan, V. Srinivasan, A. Eckhardt, M. Pollack and V. Pamula, *Lab Chip*, 2008, **8**, 2091-2104.
3. J. Kim, E. C. Jensen, M. Megens, B. Boser and R. A. Mathies, *Lab Chip*, 2011, **11**, 3106-3112.
4. Y. Oyama, T. Osaki, K. Kamiya, R. Kawano, T. Honjoh, H. Shibata, T. Ide and S. Takeuchi, *Lab Chip*, 2012, **12**, 5155-5159.
5. F. Truffer, N. Buffi, D. Merulla, S. Beggah, H. van Lintel, P. Renaud, J. R. van der Meer and M. Geiser, *Rev. Sci. Instrum.*, 2014, **85**, 015120.
6. C. D. Chin, T. Laksanasopin, Y. K. Cheung, D. Steinmiller, V. Linder, H. Parsa, J. Wang, H. Moore, R. Rouse, G. Umviligihozo, E. Karita, L. Mwambarangwe, S. L. Braunstein, J. van de Wijgert, R. Sahabo, J. E. Justman, W. El-Sadr and S. K. Sia, *Nat. Med.*, 2011, **17**, 1015-1019.
7. M. Hitzbleck and E. Delamarche, *Micromachines*, 2013, **4**, 1.
8. T. Kokalj, Y. Park, M. Vencelj, M. Jenko and L. P. Lee, *Lab Chip*, 2014, **14**, 4329-4333.
9. K. Hosokawa, M. Omata, K. Sato and M. Maeda, *Lab Chip*, 2006, **6**, 236-241.
10. I. K. Dimov, L. Basabe-Desmonts, J. L. Garcia-Cordero, B. M. Ross, Y. Park, A. J. Ricco and L. P. Lee, *Lab Chip*, 2011, **11**, 845-850.
11. M. Zimmermann, H. Schmid, P. Hunziker and E. Delamarche, *Lab Chip*, 2007, **7**, 119-125.
12. L. Gervais, M. Hitzbleck and E. Delamarche, *Biosens. Bioelectron.*, 2011, **27**, 64-70.
13. Y. Temiz, M. Lim and E. Delamarche, *Proc. Spie.*, 2016, **9705**.
14. M. S. Maria, P. E. Rakesh, T. S. Chandra and A. K. Sen, *Sci. Rep.*, 2017, **7**, 43457.
15. M. I. Mohammed and M. P. Desmulliez, *Biosens. Bioelectron.*, 2014, **61**, 478-484.
16. B. J. Yakes, S. M. Etheridge, S. P. Mulvaney and C. R. Tamanaha, *Mar. Drugs*, 2010, **8**, 565-576.
17. H. Y. Tsai, J. R. Chan, Y. C. Li, F. C. Cheng and C. B. Fuh, *Biosens. Bioelectron.*, 2010, **25**, 2701-2705.
18. O. Florescu, K. Wang, P. Au, J. Tang, E. Harris, P. R. Beatty and B. E. Boser, *J. Appl. Phys.*, 2010, **107**, 54702.
19. H. C. Tekin, M. Cornaglia and M. A. M. Gijs, *Lab Chip*, 2013, **13**, 1053-1059.
20. A. Pierres, A. M. Benoliel and P. Bongrand, *J. Biological Chemistry*, 1995, **270**, 26586-26592.
21. J. Kaur, K. V. Singh, A. H. Schmid, G. C. Varshney, C. R. Suri and M. Raje, *Biosens Bioelectron*, 2004, **20**, 284-293.
22. S. P. Mulvaney, C. L. Cole, M. D. Kniller, M. Malito, C. R. Tamanaha, J. C. Rife, M. W. Stanton and L. J. Whitman, *Biosens. Bioelectron.*, 2007, **23**, 191-200.
23. K. Y. Chumbimuni-Torres, R. E. Coronado, A. M. Mfuh, C. Castro-Guerrero, M. F. Silva, G. R. Negrete, R. Bizios and C. D. Garcia, *Rsc Adv*, 2011, **1**, 706-714.
24. A. Lamberti, S. L. Marasso and M. Cocuzza, *Rsc Adv*, 2014, **4**, 61415-61419.
25. J. M. Kim, F. Wolf and S. K. Baier, *Tribol Int*, 2015, **89**, 46-53.
26. A. J. Goldman, R. G. Cox and H. Brenner, *Chem. Eng. Sci.*, 1967, **22**, 653-660.
27. P. Schuck and H. Zhao, *Methods Mol. Biol.*, 2010, **627**, 15-54.
28. H. Bruus, *Theoretical microfluidics*, 2007.
29. Y. Z. K. Petkovic-Duran, *Microfluid. Nanofluid.*, 2009.
30. Y. J. Chuah, S. Kuddannaya, M. H. A. Lee, Y. Zhang and Y. Kang, *Biomaterials Science*, 2015, **3**, 383.
31. R. L. Rich and D. G. Myszka, *Anal. Biochem.*, 2007, **361**, 1-6.
32. K. E. Sapsford, Z. Liron, Y. S. Shubin and F. S. Ligler, *Anal. Chem.*, 2001, **73**, 5518-5524.

33. K. Wilson, D. J. Mole, N. Z. Homer, J. P. Iredale, M. Auer and S. P. Webster, *J. Biomol. Screen*, 2015, **20**, 292-298.
34. M. Zimmermann, E. Delamarche, M. Wolf and P. Hunziker, *Biomed. Microdevices*, 2005, **7**, 99-110.
35. G. Hu, Y. Gao and D. Li, *Biosens. Bioelectron.*, 2007, **22**, 1403-1409.
36. M. I. Mohammed and M. P. Desmulliez, *Lab Chip*, 2011, **11**, 569-595.
37. T. Lam, J. P. Devadhasan, R. Howse and J. Kim, *Sci Rep*, 2017, **7**, 1188.
38. J. Kim, R. Surapaneni and B. K. Gale, *Lab Chip*, 2009, **9**, 1290-1293.
39. J. Choi, A. W. Gani, D. J. B. Bechstein, J. R. Lee, P. J. Utz and S. X. Wang, *Biosens. Bioelectron.*, 2016, **85**, 1-7.
40. R. S. Gaster, D. A. Hall, C. H. Nielsen, S. J. Osterfeld, H. Yu, K. E. Mach, R. J. Wilson, B. Murmann, J. C. Liao, S. S. Gambhir and S. X. Wang, *Nat. Med.*, 2009, **15**, 1327-1332.
41. K. Skucha, S. Gambini, P. Liu, M. Megens, J. Kim and B. Boser, *J. Microelectromech. Sys.*, 2013, **22**, 1327-1338.
42. P. Liu, K. Skucha, M. Megens and B. Boser, *IEEE Trans. Magn.*, 2011, **47**, 3449-3451.
43. W. A. Bauer, M. Fischlechner, C. Abell and W. T. Huck, *Lab Chip*, 2010, **10**, 1814-1819.
44. T. Trantidou, Y. Elani, E. Parsons and O. Ces, *Microsystems &Amp; Nanoengineering*, 2017, **3**, 16091.
45. J. Kim, Y. Shin, S. Song, J. Lee and J. Kim, *Sens. Actuators, B*, 2014, **202**, 60-66.

A Capillary Flow-Driven Microfluidic System for Microparticle-Labeled Immunoassay

A simple and sensitive capillary-driven microfluidic platform is designed using newly determined interfacial coefficient and demonstrated for various types of microparticle-labeled immunoassays.